Fuel 421 (2026) 139031

Contents lists available at ScienceDirect

Fuel

journal homepage: www.elsevier.com/locate/fuel

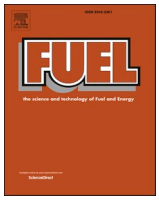

Full Length Article

Predictive combustion and knock modelling for SI engines fuelled by e-gasoline

Lorenzo Ferrari [a,*], Massimo Duchi [a], Giuseppe Sammito [b], Bartosch Jagodzinski [c], Nicolò Cavina [a]

[a] Department of Industrial Engineering, University of Bologna, Viale del Risorgimento 2, 40136 Bologna, Italy
[b] FEV Italia s.r.l, Via Livorno, 60, 10144 Turin, Italy
[c] FEV Europe GmbH, Neuenhofstraße 181, 52078 Aachen, Germany

A B S T R A C T

Synthetic fuels produced with renewable surplus electricity depict an interesting solution for decarbonising mobility and transportation applications, reducing greenhouse gas emissions and mitigating global warming. This work proposes a methodology to enable the possibility of replicating the combustion behaviour of 2 synthetic fuels: an e-gasoline fuel and MtG – E10. At first, a surrogate fuel algorithm was conceived to replicate real fuel target properties (density, C/H, RON, MON, oxygen volumetric percentage). The surrogate hydrocarbon palette was selected to represent each hydrocarbon type, and the CRECK chemical reaction mechanism was selected to define the laminar flame speeds of the surrogate composition. The methodology was developed in a 1D-CFD simulation environment, representing a single-cylinder research engine. The Eddy-Burn Up combustion model, previously calibrated for standard fossil gasoline, showed great accuracy in replicating key combustion metrics, highlighting its predictive capability without the need to recalibrate fuel-wise the turbulent flame seed parameters. The Root Mean Square Error for the maximum pressure is 1.7 bar, and the MFB50 maximum deviation is below 1°. Eventually, knock occurrence was evaluated by employing the Livengood-Wu induction time integral. The induction time integral reaches or overcomes the knocking threshold of 0.9 for most of the cases whose normalized Maximum Amplitude Pressure Oscillation 98.5 percentile value is above 1, thus showing the ability of the knock model to predict which engine operating points are knocking or not, leaving the possibility to develop control strategies based on such approach.

1. Introduction

Between 2011 and 2020, the average global temperature was 1.09°C higher than it was during the period from 1850 to 1900 [1]. This rise in temperature, known as global warming, has been linked to numerous negative effects, such as rising sea levels, melting glaciers, altered precipitation patterns, changes in the frequency of extreme weather events like flash floods and heat waves, variations in agricultural yields, and increased risks to food and water security. These impacts are often grouped under the broader term “climate change,” which represents a major threat to human society [2]. The primary driver of global warming is the buildup of greenhouse gases (GHG_s) in the Earth's atmosphere, with carbon dioxide (CO_2) having the most significant role. CO_2 is responsible for about 64% of the absorption and re-emission of infrared radiation, making it the dominant contributor to the greenhouse effect [2].

To cope with the rise of GHG emissions, the European Union (EU) has adopted one of the most ambitious climate policies, encapsulated in the legislative package termed the European Green Deal (EGD). This framework aims to achieve net-zero emissions by 2050, aligning with the Intergovernmental Panel on Climate Change (IPCC) scenario that limits global temperature increase to 1.5°C with respect to preindustrial levels [1]. From this perspective, a mid-term milestone is represented by the Fit for 55 goal, which aims to reduce GHG emissions by 55%, relative to 1990 levels, by 2030 [3]. The transport sector is responsible for 23% of GHG_s emissions, of which 73% comes from road transport, whose contribution is expected to increase faster than any other [4]. Forecasts suggest that by 2050, the number of vehicles around the globe will double [5], which represents not only a rise in the demand for mobility solutions but also a great surge in energy consumption and associated carbon emissions [6]. In the last decade, the regulations mentioned above have accelerated the transition towards Electric Vehicles (EV_s), referring to them as zero-emission vehicles. However, the zero emissions are only from the tailpipe of the vehicle, while if the overall life cycle is considered, the overall emissions are not null [7]. This does not represent an efficient way for the decarbonization of the automotive sector since electricity around the world is mostly produced from fossil fuels (such as coal, oil, etc.), which have a great impact on GHG_s emissions [8]. The EV fleet is supplied by these fossil-based power plants, which

* Corresponding author.
E-mail address: lorenzo.ferrari28@unibo.it (L. Ferrari).

https://doi.org/10.1016/j.fuel.2026.139031
Received 6 June 2025; Received in revised form 16 January 2026; Accepted 3 March 2026
Available online 9 March 2026

Nomenclature

Definitions Abbreviations

0D/1D/3D	Zero/One/Three Dimensional
AFR_s	Stoichiometric Air-to-Fuel Ratio
AKI	Anti-Knock Index
CA	Crank Angle
CHR	Carbon To Hydrogen Ratio
CFD	Computational Fluid Dynamics
COV	Coefficient of Variation
C_3H_8	Propane
CO	Carbon Monoxide
CO_2	Carbon Dioxide
DC	Distillation Curve
EGD	European Green Deal
ETRF	Ethanol Toluene Reference Fuel
EU	European Union
EV_s	Electric Vehicles
FACE	Fuels for Advanced Combustion Engines
FSN	Filter Smoke Number
GDI	Gasoline Direct Injection
GHG_s	Greenhouse Gases
HCR	Hydrogen to Carbon Ratio
HC	Unburnt Hydrocarbons
HEV	Hybrid Electric Vehicles
ICE	Internal Combustion Engine
ID	Ignition Delay
IMEP	Indicated Mean Effective Pressure
IPCC	Intergovernmental Panel On Climate Change
ITI	Induction Time Integral
IVC	Intake Valve Closing
LFS	Laminar Flame Speed
LHV	Lower Heating Value
MFB50	Angle of 50% Mass Fraction Burned
MFB1090	Angle Interval Between 10% and 90% Mass Fraction Burned
MAPO	Mean Amplitude Pressure Oscillation
MON	Motor Octane Number
MTBE	Methyl *tert*-butyl ether
MtG	Methanol-To-Gasoline
NOX	Nitrogen Oxides
O_2	Oxygen
OP	Operating Point
OS	Octane Sensitivity
PHEV	Plug-In Hybrid Electric Vehicles
PMEP	Pumping Mean Effective Pressure
PtX	Power To X
RMSE	Root Mean Square Error
RON	Research Octane Number
RPM	Revolutions Per Minute
SCRE	Single Cylinder Research Engine
SGF	Synthetic Gasoline Fuel
SI	Spark Ignited
TDC	Top Dead Center
TPA	Three Pressure Analysis
VVT	Variable Valve Timing
VO	Oxygenated Volume Fraction

Symbols

$\boldsymbol{A}$	Matrix to account for multiple species in the same class of hydrocarbon
$\boldsymbol{J}$	Cost function
$\boldsymbol{J_h}$	Target property error term
$\boldsymbol{M_C}$	Carbon molar mass
$\boldsymbol{M_H}$	Hydrogen molar mass
$\boldsymbol{M_{N_2}}$	Nitrogen molecule molar mass
$\boldsymbol{M_{O_2}}$	Oxygen molecule molar mass
$\boldsymbol{N_t}$	Number of target properties
$\boldsymbol{R^2}$	Coefficient of Determination
$\boldsymbol{T_u}$	Unburnt Mixture Temperature
$\boldsymbol{W_h}$	Target property weight
$\boldsymbol{b}$	Upper limits vector for hydrocarbon species to be included in the surrogate
$\boldsymbol{k_{MON}}$	MON tuning coefficient
$\boldsymbol{k_{RON}}$	RON tuning coefficient
$\boldsymbol{n_{C,i}}$	Species carbon atoms number
$\boldsymbol{n_{H,i}}$	Species hydrogen atoms number
$\boldsymbol{p_{cyl}}$	In-cylinder Pressure
$\boldsymbol{\nu}$	Species volume fraction vector
$\boldsymbol{\nu_i}$	Species volume fraction
$\boldsymbol{x_i}$	Species molar fraction
$\boldsymbol{\theta_{h,k,surr}}$	Surrogate general property
$\boldsymbol{\theta_{h,k,target}}$	Target general property
$\boldsymbol{\rho_i}$	Species density @ 20°C
$\boldsymbol{\rho_s}$	Surrogate density @ 20°C
$\boldsymbol{\tau_{ID}}$	Ignition Delay

have a very high carbon emission intensity. Therefore, only the tailpipe emissions (Tank-To-Wheel) of electric vehicles are zero, but the well-to-tank emissions are almost double than that of conventional diesel/gasoline fuels [9]. The main step, in the whole EV life cycle, which is responsible for the CO_2 emission, is battery manufacturing. As a matter of fact, the production of battery packs generates emissions ranging from 150 to 200 kg of CO_2 per kWh of capacity. To produce a battery pack with a capacity of around 50 kWh, around 7.5 tons of CO_2 are emitted, which is equivalent to travelling with an ICE vehicle for 83,000 km, considering the carbon dioxide emission limit imposed by the EU [10]. Additionally, the disposal of end-of-life batteries should be addressed, as the large-scale process is not yet state-of-the-art and may become cost-intensive in the future [11]. Very recently, the EU has set a 90% CO_2 target emission reduction by 2035 for passenger car vehicles, allowing internal combustion engines to still play a role beyond 2035, in addition to full electric and hydrogen vehicles. The remaining 10% needs to be compensated through the use of low-carbon steel made in the Union, or from e-fuels and biofuels [12].

The use of synthetic fuels can represent a viable mid-term solution to mitigate the rise in GHG_s emissions by replacing the currently diffused fossil-based fuels. Also known as electrofuels (e-fuels), they can be produced using renewable energy sources, acting as an energy storage means in which, for instance, solar energy is converted into chemical energy, being stored in the chemical bonds of the gas or the fuel [13]. They can be synthesised through chemical processes involving hydrogen and carbon dioxide as reactants, with electricity serving as the energy source. Since CO_2 is consumed during their production, their combustion process can be considered carbon–neutral, as the overall carbon dioxide balance is zero [14,15,16]. This process of storing energy through the synthesis of sustainable alternative fuels is commonly referred to as Power-to-X (PtX) [17]. As energy carriers, e-fuels offer many advantages with respect to batteries. For instance, the energy density is much higher and comparable to that of gasoline (46 MJ/kg compared to 0.4 – 0.65 MJ/kg of batteries) [18,19]. Moreover, electrofuels can benefit from an already existing infrastructure, making transportation and delivery easier and cheaper [13,20]. Additionally,

the drop-in capabilities of e-fuels, namely the fact that they can be employed in current ICE_s without requiring any modification, make them a complementary solution to EV_s, which could enhance a rapid reduction in GHG_s emissions [16].

On the back of the previous considerations, several studies were carried out in the literature to understand the potential and the advantages of these fuel kinds. For instance, Wouters et. al [21] experimentally investigated 5 different synthetic gasoline fuels, which can be synthesised via the Methanol-to-Gasoline (MtG) process [22], and a reference fossil gasoline. The final gasoline consists of paraffins, olefins, naphthenes and aromatics, mainly in the gasoline boiling range. Iso-paraffins are the most abundant component within the synthetic product, which can be used as a drop-in fuel when blended with an octane booster such as ethanol. The four tested fuels were MtG-alcohol blends with ethanol, methanol and butanol, and POSYN fuel was tested as well. Other studies involved the analysis of POSYN ([23,24,25]), whose composition is nearly free of aromatics, making it an attractive solution to reduce soot emissions. Rockstroh et al. [26] investigated the combustion behaviour of eight synthetic gasoline refinery blending components in a Gasoline Direct Injection (GDI) engine. A fuel-blending model was conceived to optimise a synthetic fuel blend according to user-defined performance parameters, and this kind of strategy was validated via engine test bench experiments.

As regards the combustion simulation of such sustainable fuel blends, few studies have been found in the literature addressing this matter. Rossi et al. [27] developed a surrogate fuel for POSYN and a premium gasoline fuel, Super Plus 98, with the first having a higher laminar flame speed (LFS), which results in faster combustion and reduced engine knock tendency. The development of surrogate fuel mixtures is essential in combustion simulation. They consist of hydrocarbon mixtures designed to replicate key properties of a target fuel, playing a crucial role in fuel modelling, as real fuels – such as gasoline and diesel – are complex blends composed of many hydrocarbons [28]. Consequently, representing their combustion behaviour in computational environments is challenging due to both chemical and computational constraints. In fact, predicting combustion and knock phenomena in SI engines requires detailed chemical kinetic mechanisms which encompass the intricate network of reactions describing fuel oxidation. Unfortunately, when the combustion of a fuel containing a large number of species is to be modelled, issues arise both because (i) well-established kinetic mechanisms are available only for a restricted number of compounds, and (ii) because accounting for numerous reactions leads to an impractical computational burden [28,29]. In this context, it is essential to represent the fuel characteristics that are most relevant to combustion using a surrogate blend composed of a limited number of species. The complexity of surrogates has evolved over the years, starting from Primary Reference Fuels (PRF) [30], which aim to replicate the Research Octane Number (RON) of real fuel, progressing to Toluene Reference Fuels (TRF) [31] and Ethanol Toluene Reference Fuels (ETRF) [32] to also reproduce octane sensitivity, and ultimately to multi-component chemical compositions [33]. Fontanesi et al. [34] studied the effect of fuel surrogate formulation on the ability to forecast the statistical occurrence of knock in a direct injection spark-ignited optical engine. 2 surrogate fuel formulations were conceived: a 6-component surrogate fuel, including one hydrocarbon for each hydrocarbon class, and an ETRF. The targeted properties by the surrogate composition include RON, Motor Octane Number (MON), LFS, H/C and O/C ratios. Knock is investigated using a proprietary statistical knock model, which can infer the probability of knocking events within a RANS formalism, and they proved that, by a combination of laminar flame speed correlations, ignition delay look-up tables, the percentage of knocking cycles in a 3D CFD environment is well estimated, with limited computational cost. In this regard, LFS correlations are widely adopted to reduce the combustion simulation efforts rather than solving the chemical kinetics at runtime. Power-law methods ([35,36]) were developed decades ago, and it has been reported that they generally fail to predict LFS under lean and rich conditions [37]. To solve this issue, more advanced correlations have been proposed, like those of Del Pecchia et al. [38], D'Adamo et al. [39], or Sok et al. [40], with the purpose of being integrated into both 1D and 3D CFD codes for combustion simulations.

In this study, a novel methodology is presented that enables the prediction of synthetic fuels' combustion behaviour, filling the gap in the current literature to the authors' knowledge. Specifically, 2 fuel kinds, namely a synthetic gasoline fuel (SGF) and MtG-E10, were addressed. Experimental data were acquired at the engine test bench for a single-cylinder research engine (SCRE) by FEV Europe GmbH, and based on the fuel properties, a surrogate fuel algorithm was implemented to come up with an equivalent fuel with a known chemical composition. The target properties and the palette components were selected after a literature analysis to find out which of them were targeted most frequently. LFS and ignition delays (ID) of the 2 fuels were simulated via chemical kinetics employing the surrogate fuel compositions. The LFS were integrated into the 1D CFD simulation environment, representative of the SCRE, via machine learning methods, specifically via the usage of neural networks, rather than relying on LFS correlations. Another novelty relies on the use of a previously calibrated combustion model for standard fossil gasoline, extended, in this work, to synthetic fuels combustion analysis. In this regard, the 0D Eddy-Burn Up combustion model was not recalibrated in its turbulent flame speed parameters according to the specific fuel, and the flame front evolution fuel-wise was characterised through LFS neural networks developed via chemical kinetics simulations. Moreover, a 0D knock model, based on the Livengood-Wu induction time integral (ITI) [41], is integrated via a custom Python function into the 1D CFD simulation framework in order to reproduce the knocking trend of the fuels under analysis. The present authors are aware of the fact that knock is a complex phenomenon and its simulation poses several challenges, especially in a 0D framework. Nevertheless, the adopted methodology allows capturing the different behaviours related to the knock occurrence among different surrogate fuel compositions, which enables the development of virtual calibration workflows or real-time control-oriented modelling.

This work is organised as follows: Section 2 presents the experimental setup used for the data gathering, while Section 3 describes the surrogate fuel estimation algorithm. Section 4 highlights the results regarding the fuel surrogate algorithm performance, along with the methodology followed to simulate the laminar flame speeds and ignition delays of the fuels under analysis. Moreover, the results of the predictive combustion model and the knock prediction model will be shown as well.

2. Experimental setup

The experimental data for this study were provided by FEV Group GmbH. A single-cylinder research engine was utilised for data acquisition, and the main engine characteristics are reported in Table 1.

Table 1
HELEN engine hardware specifications.

Engine type	Single-cylinder, 4-stroke
Piston	Flat
Combustion chamber	Hemispherical
Displaced volume	500 cc
Stroke x Bore	113.2 x 75 mm
Stroke/Bore ratio	1.51
Connecting rod length	220 mm
Crank radius	56.6 mm
Compression ratio	Adjustable, (10.8:1, 12.2:1, 15:1)
Number of valves	4
Injection type	Direct
Valve timing	Variable
Max. peak cylinder pressure	180 bar
Max. fuel pressure	200 bar
Fuel injector	6-hole solenoid

The selected compression ratio for this analysis was 10.8:1 and, moreover, the engine could be operated with a variable valve timing (VVT) system. For fuel injection, a centrally mounted six-hole solenoid-actuated series production injector was employed, together with an intake stroke injection strategy to attain homogeneous operation. Moreover, the cylinder was equipped with a centrally mounted spark plug, and two piezoelectric transducers for the in-cylinder pressure measurement were oppositely mounted between the intake and exhaust valves. The intake and exhaust manifolds were fitted with pressure transducers as well. A hot-film air mass meter was used to measure the intake air mass flow, while a Coriolis-type mass flow sensor measured the fuel mass flow. To keep the imposed engine speed and load, the engine was coupled with an electric dynamometer and an eddy-current brake, respectively. To maintain the desired delta pressure between intake and exhaust, an external boosting system and an exhaust gas backpressure control valve were employed. For the exhaust gas components measurement (HC, CO, CO_2, NO_X, O_2), a partial exhaust gas mass flow was utilized to sample the species upstream of the backpressure control valve. Soot emissions were quantified by the filter smoke number (FSN) and measured downstream of the backpressure control valve. Eventually, HC emissions were measured as C_3H_8. A detailed description of all the measurement systems, with their respective measurement ranges and accuracies, is given in Table A.1 in the Appendix [21]. 200 cycles were recorded for each engine operating point (OP), and the mean quantities were used as input data for the present analysis.

As mentioned in the Introduction section, two synthetic fuels were tested, and their characteristics are reported in Table 2. It is worth noting that the SGF is almost free of aromatics and olefins, and it has a higher RON and MON than the MtG-E10, which can be regarded as the synthetic counterpart of the standard fossil gasoline.

As for the experimental data collection, the tested engine OP for MtG – E10 are reported in Table 3. Instead, for the SGF, a wider range of the engine map was investigated: load variation tests were carried out from 1500 to 2500 RPM up to 21 bar IMEP and another engine OP was tested at 2500 RPM, 16 bar IMEP (Fig. 1). For the lambda variation test, just the one at stoichiometric conditions was chosen to align the analysis with the other fuel.

In the next section, the algorithm employed to generate the surrogate fuel composition will be introduced, together with the species included in the surrogate palette and the fuel target properties to be reproduced by the surrogate composition.

Table 2
Investigated fuel properties.

Property	SGF	MtG – E10
C-content [% m/m]	82.18	82.85
H-content [% m/m]	15.15	13.52
O-content [% m/m]	2.67	3.63
Density @ 15°C [kg/m^3]	723.00	744.10
Lower heating value [MJ/kg]	42.84	41.40
Molar mass [g/mol]	92.40	88.20
RON/MON [-]	100/91	96.6/85.9
Vapor pressure DVPE [kPa]	46.60	71.50
C/H/O mass share [-]	6.3/13.9/0.15	6.08/11.83 /0.2
Air-to-fuel ratio [-]	14.50	14.02
Aromatics [% V/V]	< 0.5	30.60
Olefines [% V/V]	< 0.5	4.14
Saturated hydrocarbons [% V/V]	85.10	55.26
Alcohols [% V/V]	14.40	10.00

Table 3
Investigated engine OP for MtG − E10.

Engine speed [1/min]	IMEP [bar]	EGR [%]	Fuel
2500	16	0–25	MtG – E10
2500	3–21	0	MtG – E10

3. Surrogate fuel algorithm

3.1. Fuel properties

In general, target properties can be classified as either chemical or physical. Their selection is not standardised and depends on the specific application and operating conditions to be simulated [33]. Density, viscosity and volatility are particularly important when simulating in-cylinder flow, spray formation and mixture behaviour, as in 3D CFD modelling of GDI applications [42,43]. On the other hand, chemical properties remain crucial even when the spatial resolution of flow and combustion is negligible, as in the lumped parameters approach. This is because air–fuel mixture oxidation is inherently governed by the fuel's molecular structure [33], whose influence is evident in zero-dimensional models describing turbulent combustion in SI engines, where the laminar flame speed is a key parameter [44]. The latter can be computed by chemical kinetics simulations employing chemical reaction mechanisms, which detail the transformation of reactants into products, accounting for intermediate species formation, consumption, and the associated heat release [33]. Typical chemical properties are RON and MON, which represent the standardised indexes ([45,46]) of the fuel resistance to autoignition, responsible for the knock phenomenon in SI engines [47]. Another key chemical property for fuel characterisation is the Carbon-to-Hydrogen ratio (CHR). This parameter represents the proportion of carbon to hydrogen atoms within the fuel and is thus closely connected to its overall chemical structure. It is also related to other important fuel properties, such as density, Lower Heating Value (LHV), as shown in Fig. 2, and combustion characteristics, including flame propagation and flame temperature [29]. Additionally, this quantity is linked to the mixture's stoichiometric air–fuel ratio (AFR_s). As the stoichiometric fuel chemical reaction (Eq. (1)) shows [48], there is a clear link between the CHR and the AFR_s (Eq. (2)). In the latter Equation, M_{O_2}, M_{N_2}, M_C, and M_H are the molar masses of the respective molecules.

$$C_xH_y + \left(x+\frac{y}{4}\right)\left(O_2+\frac{79}{21}N_2\right) \rightarrow xCO_2 + \frac{y}{2}H_2O + \frac{79}{21}\left(x+\frac{y}{4}N_2\right) \quad (1)$$

$$AFR_s = \frac{\left(\frac{x}{y}+\frac{1}{4}\right)\left(M_{O_2}+\frac{79}{21}M_{N_2}\right)}{\frac{x}{y}M_C + M_H} \quad (2)$$

Additionally, the amount of oxygenated compounds in the fuel plays a crucial role. For instance, ethanol is usually blended with gasoline-like fuels to enhance performance and reduce emissions. The efficiency gains associated with ethanol-blended gasoline arise from its high antiknock quality, which allows for near-optimal spark timings across a broader range of operating conditions and enables the use of higher compression ratios, thereby improving engine thermodynamic efficiency. Moreover, the presence of oxygenates in the fuel contributes to emissions reduction, as they decrease the fuel's tendency to produce soot, HC, and CO emissions. However, oxygenated fuels present a lower heat of combustion since the oxygen present in the fuel does not take part in the combustion process [38,49,50].

In the literature, several surrogate fuel formulations have been developed by analysing different kinds of gasoline-like fuels. Surrogates for two Fuels for Advanced Combustion Engines (FACE) are proposed in [29], along with a surrogate for a typical Eurosuper fuel. In addition, the study presented in [42] focuses on replicating key characteristics of FACE A and FACE C fuels. The selected target properties include the Hydrogen-to-Carbon Ratio (HCR), liquid density, RON, compositional characteristics, and the distillation profile. While the HCR and density are estimated using linear blending rules, the surrogate's RON is evaluated by running a chemical kinetic model at each optimisation step to

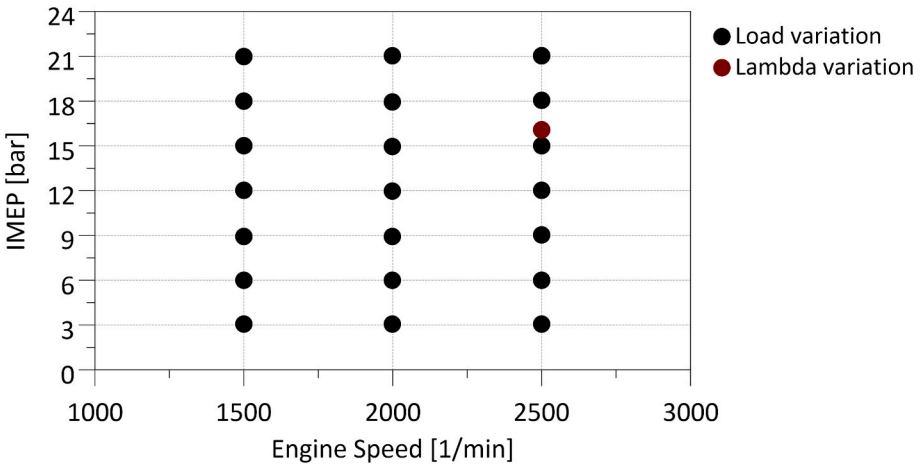

Fig. 1. Synthetic Gasoline Fuel engine OP under analysis.

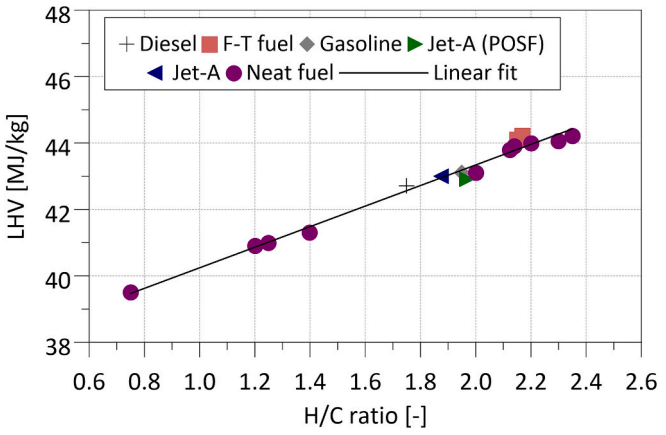

Fig. 2. Correlation between LHV and Hydrogen to Carbon ratio for different real fuels (.
adapted from [33])

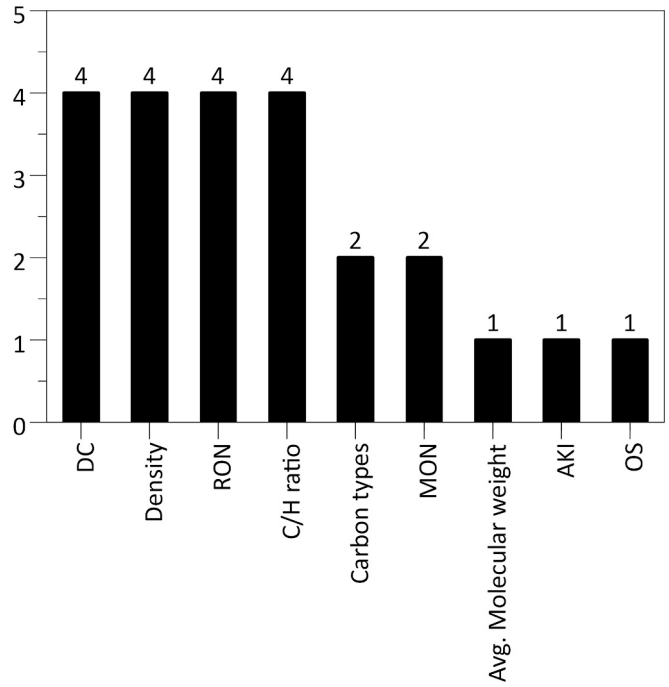

Fig. 3. Target properties for surrogate generation algorithm in [42,29,52,53].

calculate the ID time of the corresponding mixture composition. A correlation between ID and RON is then used to estimate the surrogate's octane rating. The simulation tool REFPROP [51] is employed to estimate the surrogate's distillation curve (DC) based on a physical model implemented within the tool. Fig. 3 sums up the frequency whereby, in the considered studies, a certain fuel property has been targeted to generate the surrogate composition.

From the above literature analysis, in this work, the selected target properties include fuel liquid density, CHR, RON and MON, and the volume fraction of oxygenates. In the next section, the main compounds used to generate the surrogate will be discussed, along with the modelling of the selected target properties.

3.2. Target chemical species

Fuel combustion behaviour is also influenced by its chemical composition, which impacts several combustion-significant parameters, such as volatility, ignition delay, vaporisation and heat release [42]. Hydrocarbons present in gasoline-like fuels can be distinguished into five main classes, namely n-Paraffins, Iso-paraffins, Olefins, Naphthenes and Aromatics. This classification depends on the nature of the chemical bonds between hydrogen and carbon atoms, as well as on the molecular structure. When the composition of a fuel is expressed in terms of its hydrocarbon classes, it is referred to as the PIONA composition. Fig. 4 depicts molecular structures of chemical species representative of the different PIONA categories.

N-paraffins, or n-alkanes, are linear saturated hydrocarbon chains, represented by the general formula C_nH_{2n+2} and characterised by low octane ratings. Due to this characteristic, n-alkanes are present in gasoline fuels in a very low share, usually below 1% [33]. On the other hand, isoparaffins have the same general formula as paraffins but present methyl substitutions, which result in a branched molecular structure. This increases the anti-knock quality of this class of compounds, and a larger fraction of gasoline-like fuels is constituted by them [33]. Naphthenes are *cyclo*-alkanes, represented by the formula C_nH_{2n}. Their octane quality is low, and therefore, their presence in real gasoline fuels is limited to below 20% in volume. Common naphthenes found in gasoline are cyclopentane and cyclohexane [33]. Olefins are alkenes, characterised by double bonds in their molecular structure, which can be summarised as C_nH_{2n}. Double bonds confer high octane ratings; however, they are limited to fractions below the 18% volume in market-grade gasoline fuels [52], due to their poor oxidative stability, which reduces fuel storage life [33]. As for aromatics, they are the highest molecular weight components found in real gasoline. They increase the

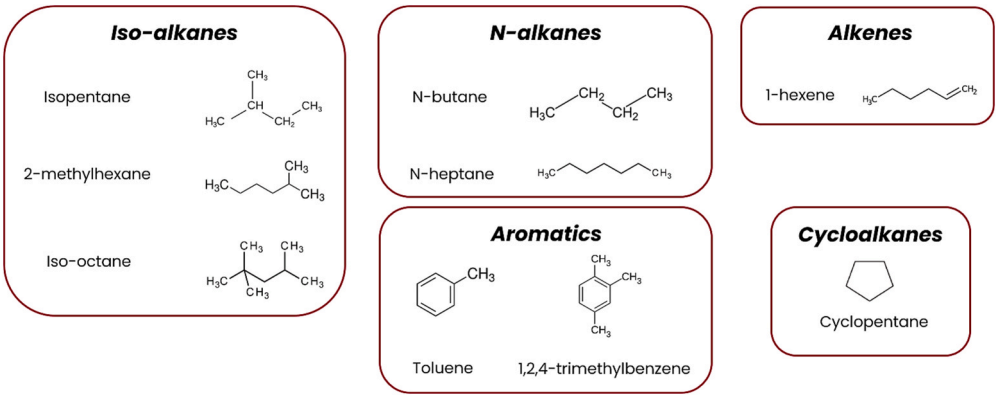

Fig. 4. Molecular structures of gasoline components representative of the PIONA classes (adapted from [52]).

high-temperature tail-end of the DC but enhance soot formation, so their share is limited to below 35% volume by the EN 228 standard [52]. The most aromatic compounds found in gasoline are alkylbenzenes, such as toluene [33]. Eventually, commercial gasoline is typically blended with

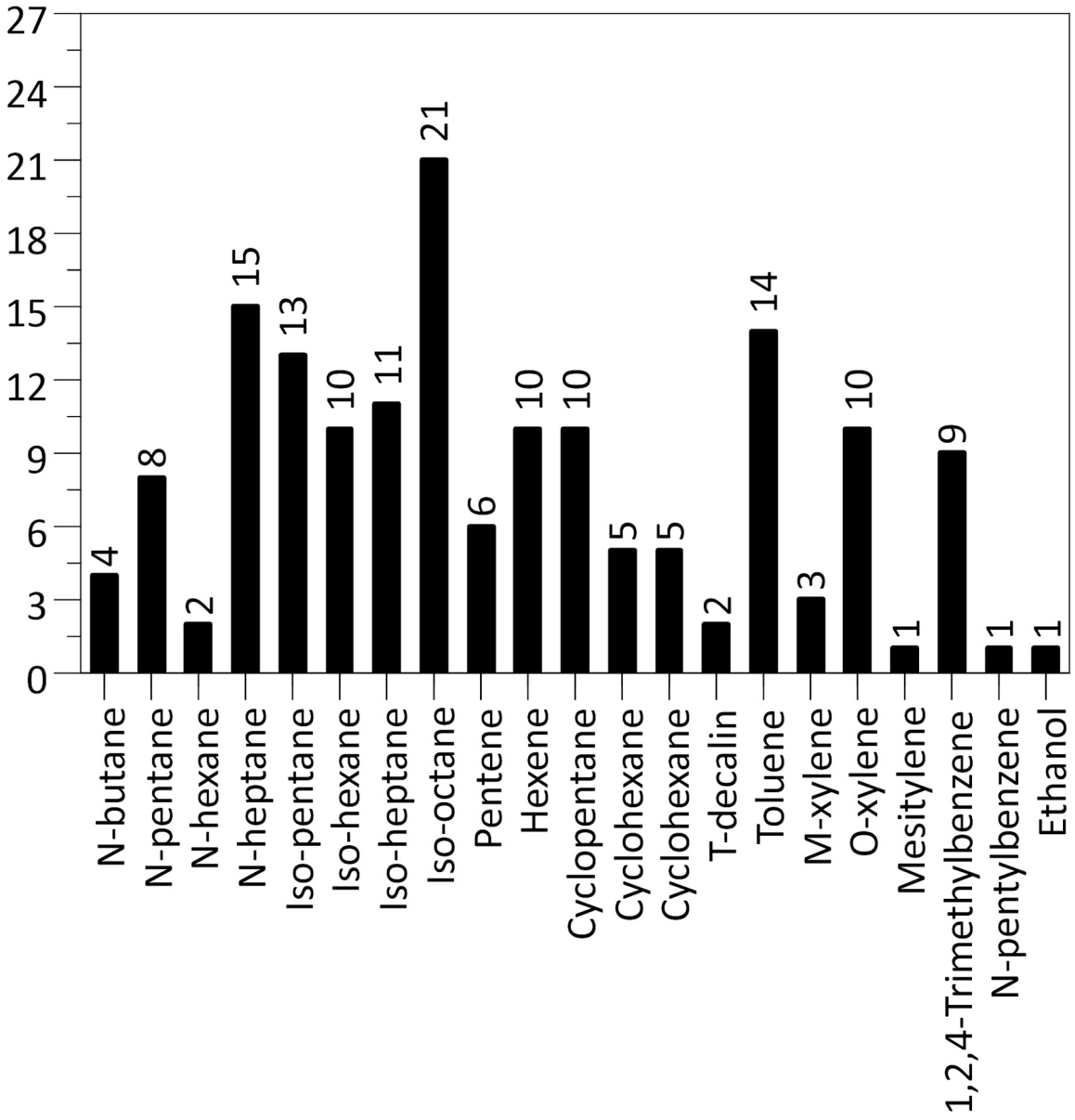

Fig. 5. Selected chemical species for surrogate generation algorithm in [42,29,52,53].

oxygenated compounds such as ethanol [38]. Therefore, it is reasonable to include the oxygen volume fraction among the properties that a valid fuel surrogate should accurately replicate. It is worth highlighting here that the kind of oxygenates plays a crucial role in the determination of the AFR_s and LHV of the surrogate fuel. As already mentioned in Section 3.1, the presence of oxygen in the fuel reduces the AFR_s and the LHV, but its sensitivity depends on the kind of oxygenates present in the fuel composition. To provide an example, methyl *tert*-butyl ether (MTBE) has an oxygen mass share in its molecule of 18%, while ethanol, an alcohol, of 35%. Therefore, the same amount of oxygenates has a different impact on the AFR_s and LHV reduction. In this study, the surrogate fuel algorithm is designed for a general application, and the present authors decided to use ethanol as oxygenates representative to be included in the surrogate chemical species palette. Being the AFR_s and the LHV not targeted by the algorithm, deviations are expected with respect to fuels which do not contain alcohols in their real chemical compositions.

When it comes to the surrogate components selection criteria, as the number of selected chemical and physical target properties increases, more complex surrogates are required to achieve sufficiently close values for these characteristics [43]. However, surrogates are used in detailed chemical kinetic mechanisms to compute combustion-relevant parameters such as ignition delay or laminar flame speed. Since the computational expense of these calculations scales with the square of the number of species in the surrogate [43], increasing the number of palette components significantly raises the computational cost. Therefore, selecting a minimal yet sufficiently representative set of species that, when blended in the right proportions, form a computationally efficient yet accurate fuel surrogate is crucial. First, the thermo-physical properties of the pure components should be available in the literature to facilitate accurate mixture property estimation [43]. Additionally, each selected species must be included in a well-established and reliable chemical kinetic mechanism to enable accurate simulation of the fuel combustion process [29]. Finally, to replicate the behaviour of gasoline-like fuels, the molecular size of the chosen components should span the range of C5–C10, covering the majority of gasoline-like fuel constituents. This is particularly important when aiming to reproduce the fuel's DC, as the boiling range of hydrocarbons correlates with molecular size, and real SI engine fuels exhibit a broad distillation range, typically spanning temperatures from 25°C to 170°C [43]. By analysing the literature, several studies can be found related to the formulation of surrogate fuels. Recalling the studies of the previous section ([42,29,53,54]), the most used chemical species to come up with the surrogate composition are summed up in Fig. 5. It is worth highlighting the fact that, in these studies, several hydrocarbon palettes were utilised to generate the surrogates, so the same chemical species were counted multiple times as they appeared in more surrogate palettes.

In conclusion, in this work, the target fuel properties to be replicated by the surrogate fuel, made up of a proper combination of selected hydrocarbon species, are reported in Table 4. The species were selected as the most used ones for each hydrocarbon class.

3.3. Target properties modelling

The algorithm implemented to generate the two multi-component fuel surrogates is based on the minimisation of a cost function, which accounts for the deviation of the surrogate mixture's properties from their real counterparts. To enable cost function formulation, mixture properties – which need to be compared with real fuel ones – must be estimated.

Table 4
Target properties and selected chemical species for the surrogate palette.

Chemical species	Target properties
N-heptane	Liquid density
Iso-octane	CHR
Toluene	RON
Cyclohexane	MON
1-hexene	VO
Ethanol	

Surrogate liquid density at 20°C, ρ_s, can be modeled as [42]:

$$\rho_s = \sum_{i=1}^{N} v_i \rho_i \tag{3}$$

ρ_i, $i = 1, \ldots, N$ are pure components' liquid densities at 20°C, N is the number of species included in the palette and v_i is the volume fraction of the i-th pure component in the surrogate blend.

Analogously, the surrogate CHR, CHR_s, can be estimated as the ratio between the molar-fraction-based average carbon atoms number and the molar-fraction-based average hydrogen atoms number, namely [42]:

$$CHR_s = \frac{\sum_{i=1}^{N} x_i n_{C,i}}{\sum_{i=1}^{N} x_i n_{H,i}} \tag{4}$$

where $n_{C,i}$ and $n_{H,i}$ are the number of carbon and hydrogen atoms contained in the molecular structure of the i-th pure component, respectively, while x_i is the molar fraction of the i-th species in the mixture.

Conversely, when it comes to modelling the surrogate RON and MON, a linear mixing rule is likely to produce inaccurate results – as pointed out in [43,55] – especially if an alcohol, such as ethanol, is included in the hydrocarbon mixture. Consequently, the following mixing rule, accounting for the non-linearity of RON and MON w.r.t. alcohol molar fraction, has been adopted to model surrogate octane ratings [55]:

$$RON_s = \sum_{i=1}^{N} x_i RON_i + k_{RON} x_a (1 - x_a)(RON_a - \sum_{i=1, i\neq a}^{N} x_i RON_i) \tag{5}$$

$$MON_s = \sum_{i=1}^{N} x_i MON_i + k_{MON} x_a (1 - x_a)(MON_a - \sum_{i=1, i\neq a}^{N} x_i MON_i)$$

Here RON_s and MON_s are RON and MON estimations for the surrogate, respectively, while RON_i and MON_i are RON and MON of the i-th pure component, respectively. Additionally, in Eq. (5), a is the index associated with the oxygenate present within the palette – i.e., $i \equiv a$ when the i-th pure component considered is ethanol, in this case – while $k_{RON} = 0.45$ and $k_{MON} = 0.94$ are two tuning coefficients, whose values have been defined according to [55,56].

Since the optimisation process depends on volume fraction composition as the optimisation variable, the calculation of the VO present within the surrogate can be directly performed by the summation of the volume fractions associated with oxygenates present within the palette.

3.4. Optimisation scheme

The objective of the surrogate generation algorithm is to determine the optimal surrogate composition that best matches the estimated surrogate properties with those of the real fuel. To achieve this, an optimisation scheme is implemented based on the minimisation of a cost function, J. This cost function quantifies the deviation of the surrogate properties from their respective target values. By assigning an index $h = 1, \cdots, N_t$ to each target property, J can be expressed as:

$$J = J(\mathbf{v}) = \sum_{h=1}^{N_t} W_h J_h(\mathbf{v}) \tag{6}$$

Here, J_h represents the h-th error term, quantifying the deviation of the h-th surrogate property from its corresponding target value. The array $\mathbf{v} = [v_1, \ldots, v_N]$ collects the volume fractions of the palette species in the surrogate, while W_h is the weight assigned to J_h. The error term for a general h-th target property can be expressed as:

$$J_h(\mathbf{v}) = \frac{1}{N_{data,h}} \sum_{k=1}^{N_{data,h}} \left(\frac{\theta_{h,k,surr}(\mathbf{v}) - \theta_{h,k,target}}{\theta_{h,k,target}} \right)^2 \quad (7)$$

Here, k is the index associated with the number of data points, $N_{data,h}$, available for the h-th target property, while $\theta_{h,k,surr}$ and $\theta_{h,k,target}$ represent the values of the h-th target property at the k-th data point for the surrogate and target fuel, respectively. This formulation allows for the inclusion of properties with multiple data points.

The cost function weights determine the priority assigned to each target property: generally, a higher weight leads to a more accurate reproduction of the corresponding target property. In this work, the algorithm used for surrogate generation assigned equal weights (set to unity) to all target properties, ensuring uniform relevance across them. At this point, the optimisation problem can be formulated as:

$$\min_{\mathbf{v} \in \mathbb{R}^N} J(\mathbf{v}), s.t. \begin{cases} v_i \geq 0, \forall i = 1, \cdots, N \\ Av \leq b \\ \sum_{i=1}^{N} v_i = 1 \end{cases} \quad (8)$$

The optimisation problem defined in Eq. (8) is subject to an equality constraint, $\sum_{i=1}^{N} v_i = 1$, imposed by the total volume balance of the surrogate, a lower boundary set to zero for all the components' volume fractions, and an inequality constraint, $\mathbf{Av} \leq \mathbf{b}$. The inequality constraint ensures that the resulting surrogate fuel is a drop-in replacement of gasoline, complying with the EN 228 standard [52], regarding the allowable content of olefinic, aromatic, and oxygenated hydrocarbons. To formulate the surrogates, the constrained optimisation problem defined by Eq. (8) is solved using Matlab's Global Search algorithm. This algorithm, described in [57], is available in the Global Optimisation Toolbox and aims to identify the global minimum of the cost function.

3.5. Fuel combustion modelling methodology

See Fig. 6 highlights the methodology that was followed to carry out the analysis. Starting from an existing 1D CFD model, representative of the single-cylinder research engine employed in this study, whose combustion model was previously calibrated for standard fossil gasoline, the results from the surrogate fuel algorithm were utilised to model the combustion of the fuels under analysis. In particular, the surrogate formulations were defined in the GT-Suite simulation environment as fluid mixtures, and to come up with reference burn rate profiles to be compared to those predicted by the combustion model, the Three-Pressure-Analysis (TPA) was carried out. This kind of simulation takes experimental boundary data like the in-cylinder pressure, the intake and exhaust port pressures, the valve lifts/timings, the tumble coefficients, the spark timing, the boundary intake and exhaust temperatures and the intake EGR fraction to estimate the in-cylinder conditions at intake valve closing (IVC). Another crucial input for the TPA is the 0D in-cylinder turbulence model, which was already calibrated by the present authors during the first time tuning of the 0D combustion model. In particular, the results from the 3D CFD cold flow simulations were employed to calibrate the already embedded 0D turbulence model into GT-Suite, specifically regarding the turbulent kinetic energy and the integral length scale profiles. Other outputs of the TPA are the fuel burn rate and the simulated in-cylinder pressure when the estimated burn rate is imposed in the model. The results of the Three-Pressure-Analysis will serve to initiate the closed-volume analysis simulation in terms of trapped in-cylinder mass and turbulence level, in order to proceed and only assess the 0D Eddy-Burn Up combustion model.

Subsequently, the surrogate formulations, generated using the algorithm introduced in Sections 3.3-3.4, were employed to perform chemical kinetics simulations, providing an estimation of the laminar flame speed and ignition delay at engine-relevant thermodynamic conditions. The results were then used to generate custom LFS metamodels (neural networks), which were integrated into the "EngCombSIturb" combustion model template. It is widely acknowledged that the combustion in an ICE occurs in the so-called "wrinkled or corrugated flamelet" regimes ([32,39,58,59]), in which the flame front thickness is smaller than the lowest turbulent length scale (Kolmogorov scale). This implies that the turbulence does not change the inner flame structure, and the laminar flame speed synthesises the chemical kinetics occurring within the flame front. As for the ignition delays, a custom Python function was integrated into the model to interpolate at runtime the ID of the air–fuel mixture into the cylinder. The ID_s were employed to calculate the Livengood-Wu [41] ITI to assess the knock occurrence. This parameter is defined according to Eq. (9), and if the integral at the end of the combustion phase overcomes a user-defined threshold (0.9 in this study), the simulated engine operating point is considered as a knocking one. The threshold was reduced from 1 to 0.9 because the simulation results pertain to a mean cycle, and the combustion coefficient of variation (COV) is not modelled. On the contrary, if the COV is taken into account and the faster cycles are simulated, the knocking ITI threshold would be set to 1, meaning that the autoignition speed of the unburned gases is higher than the flame front propagation.

$$ITI = \int \frac{1}{\tau_{ID}} dt \quad (9)$$

In the next section, the results from the surrogate fuel generation algorithm will be introduced, along with the application of the surrogate fuel

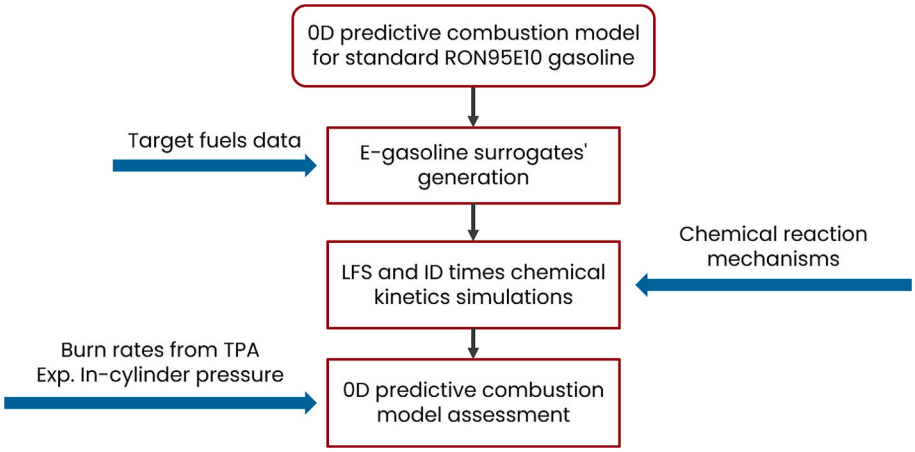

Fig. 6. Activity workflow methodology.

formulation to the predictive combustion model by the estimation of the laminar flame speeds and ignition delays at engine-relevant conditions.

4. Results and discussions

4.1. Surrogate fuel compositions

By providing the characteristics of the two multi-component fuels (SGF and MtG – E10), addressed in this work, as input target properties to the surrogate generation algorithm, two surrogate fuel formulations were obtained, and their chemical compositions are reported in Table 5. For the SGF, the cyclohexane is not targeted by the optimisation algorithm, and a higher concentration of *iso*-octane is employed, since it has a RON and CHR close to the target one. On the other hand, for the MtG – E10 fuel, more toluene is utilised to increase the overall density of the surrogate fuel with respect to the target one. Moreover, the ethanol content is determined by the algorithm to replicate the amount of oxygenates found in the real fuels.

Eventually, in Tables 6 and 7, surrogate fuel properties are compared to their real counterparts.

As can be seen, the MtG – E10 surrogate is able to reproduce all the target properties accurately, while for the SGF, the stochiometric AFR and the LHV (which are not considered as target properties by the algorithm) are affected by some deviations. The reason behind this is related to the different nature of the oxygenated compound found in the SGF. Rather than being an alcohol, it is an ether, which has a higher CHR than ethanol. That is why, recalling Eq. (2), the AFR_s and the LHV are lower if ethanol is considered as the oxygenate in the surrogate palette when the VO is correctly matched. In addition, the presence of oxygenates in fuels decreases the LHV because fuel-bound oxygen does not burn to generate heat [33]. Despite the fact that the SGF contains more oxygenate volume fraction, the presence of an ether instead of an alcohol leads to a lower impact of the oxygenate on the LHV reduction since the average oxygen mass percentage in the ether is less than that of ethanol. The lower AFR_s of the SGF surrogate lead to a reduced air requirement for the same amount of injected fuel. As a matter of fact, the overall combustion simulation is run with the same experimental injected fuel amount while the air flow rate is adjusted in a closed loop to meet the stoichiometric lambda. Moreover, the LHV may have an impact on the resulting surrogate LFS, as proven by Sileghem et al. [60], who highlighted that the energy fraction mixing rule, based on the LHV of the pure components, is the most suitable for defining surrogate gasoline mixtures' laminar flame speeds. Ethanol has almost 23% lower LHV than the corresponding ether present in the real SGF, but its LFS is considerably higher than that of ethers, as reported by Hu et al. [61]. Therefore, the 2 effects are expected to compensate each other to some extent for the SGF LFS.

Subsequently, the surrogate fuel formulations were employed to perform the three-pressure analysis, introduced in the next section, to come up with reference burn rate profiles and in-cylinder IVC conditions.

4.2. Three-pressure analysis

As previously mentioned, TPA is a crucial step in the analysis since, on one hand, it allows the validation of the experimental data acquisition and, on the other hand, it enables the possibility to estimate in-cylinder IVC conditions to subsequently perform the predictive combustion model assessment via a closed volume analysis. Fig. 7 depicts an example of the in-cylinder pressure coming from the TPA for the MtG – E10 surrogate fuel, along with the estimated burn rate profile, which best matches the experimental pressure curve. The simulated pressure profile is obtained by imposing the estimated burn rate profile in the 1D CFD model. Moreover, consistency checks, mainly related to the LHV multiplier, have been addressed by adjusting the in-cylinder convection heat transfer multiplier. The estimated burn rates will represent the reference profiles that the predictive combustion model should replicate.

Additionally, Fig. 8 highlights the TPA outcomes in terms of main combustion metrics such as Indicated Mean Effective Pressure (IMEP), Pumping Mean Effective Pressure (PMEP), maximum in-cylinder pressure, CA at the maximum pressure, MFB50, MFB1090, volumetric efficiency, air and fuel mass. As can be seen, all the addressed quantities are well reproduced by the TPA, underscoring the 1D CFD model's fidelity. As for the air mass, a higher deviation can be noticed, since the fuel flow rate is imposed in the model, while the mean intake manifold pressure is adjusted to meet the stoichiometric air-to-fuel ratio. Therefore, the Root Mean Square Error (RMSE) for the air mass is higher. Anyway, if the mean percentage error is addressed, the air flow maximum deviation is always below 5%.

Once reference burn rate profiles have been estimated, the next step is represented by the generation of fuel-specific laminar flame speed values to be then integrated into the predictive combustion model. In the following section, the methodology to achieve this end will be described and discussed.

Table 5
Fuels' surrogate chemical compositions.

Chemical species	SGF [vol. %]	MtG – E10 [vol. %]
Iso-octane	68.992%	39.300%
N-heptane	4.758%	7.200%
Toluene	6.964%	22.095%
Cyclohexane	0.000%	5.206%
1-hexene	5.277%	16.200%
Ethanol	14.009%	10.000%

Table 6
MtG − E10 surrogate properties comparison with real fuel ones.

Property	MtG – E10	MtG – E10 surrogate	Error [%]
Density [kg/m^3]	739.600	743.367	0.509
CHR [-]	0.514	0.517	0.522
RON [-]	96.600	96.546	−0.055
MON [-]	85.900	86.836	1.090
VO [-]	0.100	0.100	0.000
AFR_s [-]	14.020	13.926	−0.670
LHV [MJ/kg]	41.400	41.585	0.446

Table 7
SGF surrogate properties comparison with real fuel ones.

Property	SGF	SGF surrogate	Error [%]
Density [kg/m^3]	718.400	719.030	0.088
CHR [-]	0.453	0.453	−0.041
RON [-]	100.000	100.077	0.077
MON [-]	91.000	90.922	−0.086
VO [-]	0.140	0.140	−0.004
AFR_s [-]	14.504	13.968	−3.700
LHV [MJ/kg]	42.840	41.377	−3.416

4.3. Laminar flame speed neural network development

By following the approach of Del Pecchia et. al [38], the thermodynamic conditions to be used to perform chemical kinetics simulation for the LFS estimation were defined following a polytropic law, linking the unburnt mixture temperature, T_u, to the in-cylinder pressure, p_{cyl}. As shown in Fig. 9, both for SGF and MtG – E10, high-pressure and low-temperature grid points were not simulated, since it is unlikely that an engine will operate in such conditions. The LFS were estimated by employing the surrogate fuel formulations reported in the previous section and the CRECK chemical reaction mechanism featuring 356 species and 10,171 reactions [62]. The overall thermodynamic

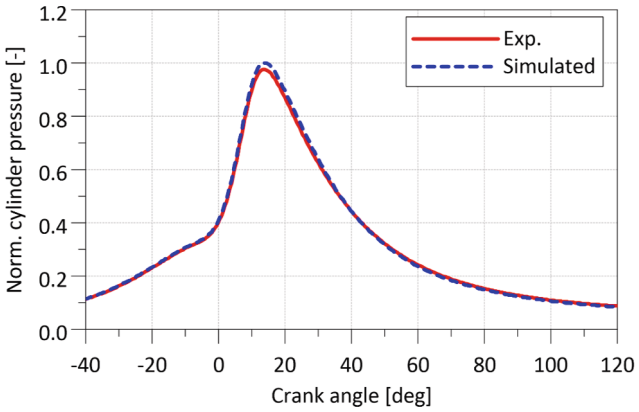

a. Normalised simulated and experimental in-cylinder pressure (MtG – E10 surrogate fuel, 2500 RPM, 12 bar IMEP, 0 % EGR)

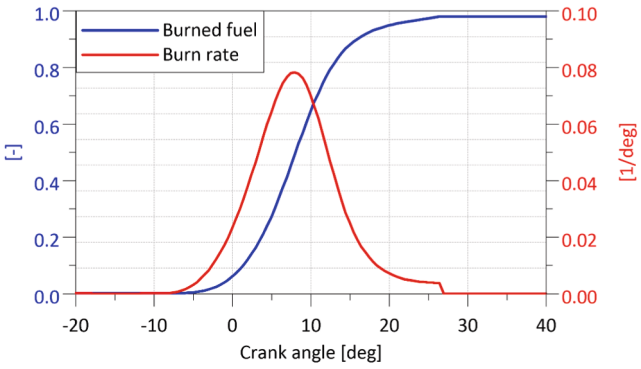

b. Reference burn rate profile from TPA (MtG – E10 surrogate fuel, 2500 RPM, 12 bar IMEP, 0 % EGR)

Fig. 7. Three Pressure Analysis outcomes.

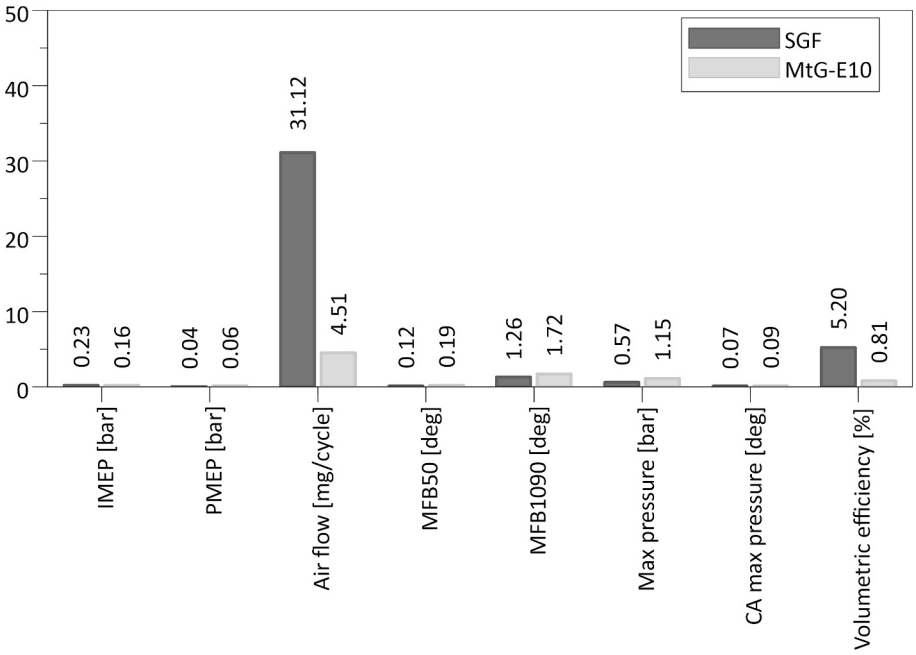

Fig. 8. TPA Root Mean Square Error with respect to experimental data.

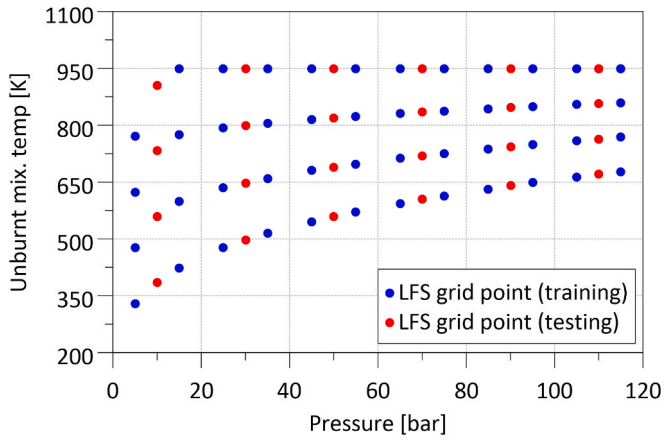

Fig. 9. LFS design of experiment for neural network metamodel generation.

conditions employed for LFS simulations, both for LFS neural network training and testing, are reported in Tables 8-9. The chemistry tool embedded in the Converge software was used to solve the chemical kinetics simulations [63].

Once the laminar flame speed values were computed for both investigated fuels, the GT-Post metamodel generator tool was employed and fed with the computed LFS. The input features to train the network are the same as the ones used for the chemical kinetics simulations, and the output response is the LFS at that particular engine thermodynamic condition. For each fuel, a sweep of the most important hyperparameters was performed, such as the number of hidden layers, the number of neurons and the kind of hidden layer transfer functions, to choose the best neural network for predicting the testing LFS dataset. For the training, a cross-validation logic was employed using 20% of the training dataset for the network weights optimisation.

Fig. 10 depicts the performance of the neural networks featuring the highest coefficient of determination (R^2) and the lowest RMSE concerning the testing dataset. For the SGF, the best-performing neural network consisted of a single hidden layer with 5 neurons using a sigmoid activation function, while the output layer employed a linear activation function. In contrast, for MtG-E10, the metamodel also featured a single hidden layer, but with 7 neurons and the same activation functions. As can be noticed, the metamodels are quite simple in their hyperparameters, meaning that the combustion model can be tailored fuel-wise even with a very basic neural network, providing an alternative to the widely used LFS correlation available in literature, such as the Gulder [36] or the Metghalchi one [35].

All the neural networks are able to replicate the testing dataset with good accuracy. A slightly lower performance can be spotted for the SGF metamodel; the highest deviations both for the training and the testing dataset were raised for EGR greater than 20%. In the present analysis, these deviations do not represent an issue since, for the e-gasoline external EGR is not addressed, and the maximum internal EGR, encountered at the lowest load of 3 bar IMEP, is around 10%, for which the testing dataset is well predicted by the neural network.

The next section highlights the methodology employed to simulate

Table 8
In-cylinder conditions for SGF/MtG – E10 LFS training dataset.

	Pressure [bar]	Unburnt mix. T [K]	Equivalence ratio [-]	EGR [%]
Min	5	328	0.8	0
Max	115	950	1.2	30
Delta	10	4 steps for each pressure value	0.2	10

Table 9
In-cylinder conditions for SGF/MtG – E10 LFS testing dataset.

	Pressure [bar]	Unburnt mix. T [K]	Equivalence ratio [-]	EGR [%]
Min	10	385	0.9	5
Max	110	950	1.1	25
Delta	20	4 steps for each pressure value	0.2	10

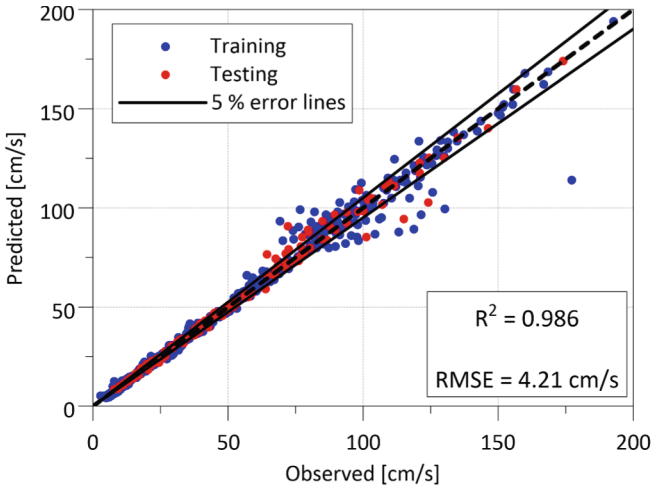

a. SGF LFS neural network performance

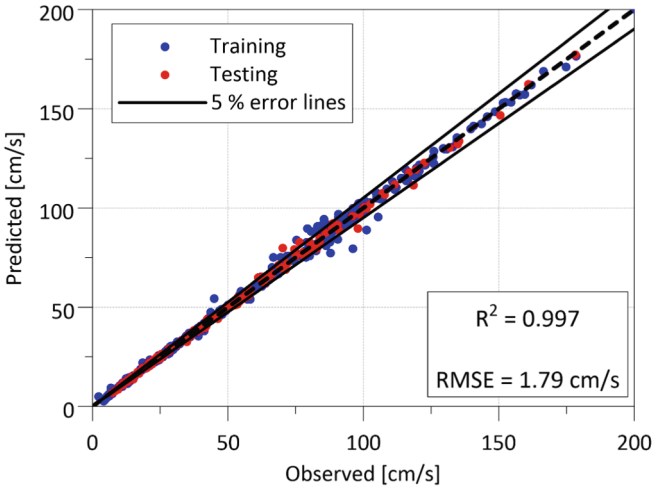

b. MtG – E10 LFS neural network performance

Fig. 10. Surrogate fuels laminar flame speed neural networks.

the fuels' ignition delays in order to compute, during runtime, the Livengood-Wu knock induction time integral [41].

4.4. Ignition delay simulations

When it comes to ignition delay chemical kinetics simulations, a simplified surrogate version of the multi-component fuels was utilised, that is, an ETRF surrogate formulation. As pointed out in several studies

([38,31,64,65,66,67,68,69]), ETRF surrogate fuels can represent with a high degree of accuracy auto-ignition delays of gasoline-like fuels.

As a consequence, the same surrogate algorithm was used to generate ETRF surrogates for the SGF and MtG – E10 fuels. Table 10 reports the composition of the ETRF surrogates, while Tables 11-12 compare the ETRF surrogate properties with real fuel ones. Even with a simplified hydrocarbon palette, the ETRF surrogate can replicate the real fuel target properties with high fidelity. A slightly worse property matching can be observed for both surrogates when compared to the complete palette surrogate ones. The same considerations mentioned in the surrogate fuel compositions section, related to the SGF AFR_s and LHV, also apply to this surrogate kind.

The ETRF fuel formulations were utilised to perform 0D constant volume chemical kinetics simulations, with the Converge software [63], to estimate the auto-ignition time. Specifically, the auto-ignition time is defined as the time interval between the start of the simulation and the temperature rising by 400 K above the initial value. Table 13 reports the thermodynamic conditions considered to perform such simulations for MtG – E10 and SGF.

Given the thermodynamic conditions and the fuel chemical compositions, the ignition delays were simulated by using the reduced LLNL chemical reaction mechanism featuring 312 species and 2469 reactions [70]. The ID grid was interpolated at runtime via a Python script, and the induction time integral was then computed by using Eq. (9). In the next section, the predictive combustion model performance will be assessed, along with the knock prediction model.

4.5. Combustion model assessment

In order to assess the performance of the predictive combustion model, closed-volume simulations were conducted starting from the in-cylinder IVC conditions estimated by the three-pressure analysis, as explained in Section 3.5. As a remark, the combustion model was not recalibrated from the turbulent flame speed parameters point of view, but only the surrogate fuel laminar flame speed metamodel was varied while switching the type of fuel.

Fig. 11 depicts the in-cylinder pressure curves and burned fuel fraction comparisons between the predictive combustion model and the reference profiles for the 2 fuels under analysis.

From the plots, the predictive combustion model can predict the burn rate of the investigated fuels with high accuracy, even for medium EGR rates (Fig. 11e, 11f), which are critical conditions for high-temperature laminar flame speed simulations. In addition, the retarded SA cases are well captured as well (Fig. 11c, 11d, 11g, 11h).

Combustion-related metrics were evaluated against the corresponding reference values coming from TPA. Specifically, the RMSE was used to assess the performance of the combustion model. Table 14 reports the RMSE considering both fuels: as the MFB50 and MFB1090 RMSE show, the combustion phasing is overall captured, as well as the indicators regarding the cylinder pressure.

As a last analysis, in the following section, the knock prediction results, employing the induction time integral methodology, will be reported and discussed.

Table 10
ETRF surrogate fuel compositions.

Chemical species	SGF [vol. %]	MtG – E10 [vol. %]
Iso-octane	71.563%	49.365%
N-heptane	6.671%	14.504%
Toluene	7.757%	26.132%
Ethanol	14.010%	10.000%

Table 11
MtG − E10 ETRF surrogate properties comparison with real fuel ones.

Property	MtG – E10	ETRF MtG – E10 surrogate	Error [%]
Density [kg/m^3]	739.600	748.764	1.239
CHR [-]	0.514	0.517	0.557
RON [-]	96.600	95.934	−0.690
MON [-]	85.900	87.443	1.796
VO [-]	0.100	0.100	0.000
AFR_s [-]	14.020	13.930	−0.641
LHV [MJ/kg]	41.400	41.496	0.231

Table 12
SGF ETRF surrogate properties comparison with real fuel ones.

Property	SGF	ETRF SGF surrogate	Error [%]
Density [kg/m^3]	718.400	721.346	0.410
CHR [-]	0.453	0.453	−0.130
RON [-]	100.000	99.888	−0.112
MON [-]	91.000	91.109	0.120
VO [-]	0.140	0.140	0.000
AFR_s [-]	14.504	13.974	−3.564
LHV [MJ/kg]	42.840	41.353	−3.470

Table 13
SGF and MtG − E10 constant volume ignition delay thermodynamic conditions.

	Pressure [bar]	Unburnt mix. T [K]	Equivalence ratio [-]	EGR [%]
Min	5	600	0.8	0
Max	120	1000	1.2	35
Delta	5	8 steps for each pressure value	0.1	5

4.6. Knock prediction assessment

As mentioned in the Ignition Delay Simulations section, knock occurrence was evaluated by using a simplified surrogate formulation. The simulated ignition delay grid was interpolated at runtime by employing a Python script, which was integrated into the 1D CFD SCRE model. The induction time integral (Eq. (9)) was then evaluated for each engine operating condition and compared with the normalised Mean Amplitude Pressure Oscillations (MAPO) 98.5 percentile (Eq. (10)). The knock limit is defined as in Eq. (11), and it includes the effect of the engine speed on the MAPO 98.5 percentile knock limit.

$$MAPO_{norm} = \frac{MAPO_{98.5}}{Knocklimit} \tag{10}$$

$$Knocklimit = \frac{RPM}{1000} + 0.5 \tag{11}$$

Knock is experimentally detected when the normalized $MAPO_{98.5}$ value exceeds unity while, in the simulation, knock is identified when the ITI surpasses the 0.9 threshold. Fig. 12 compares the ITI with the $MAPO_{norm}$ for the investigated fuels.

For both fuels, a general agreement between the ITI and the normalised MAPO 98.5 percentile can be found. As for the synthetic gasoline fuel, cases 4–11-18 show the biggest discrepancy between the normalised MAPO 98.5 percentile. All these cases are at 12 bar IMEP, which represents, for the SCRE, the load point at which the cylinder experiences knocking onset. Above 12 bar IMEP (cases 5–6-7–12-13–14-19–20-21), the SCRE runs into knocking phenomena, or it is really close

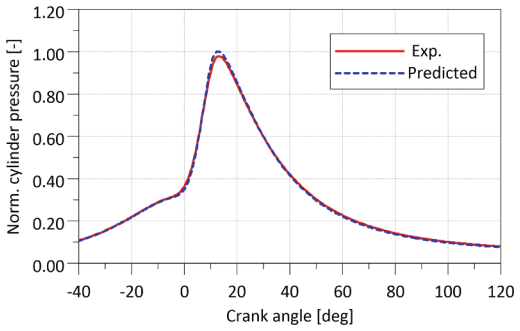

a. SGF in-cylinder pressure, 1500 RPM, 9 bar IMEP, 0% EGR

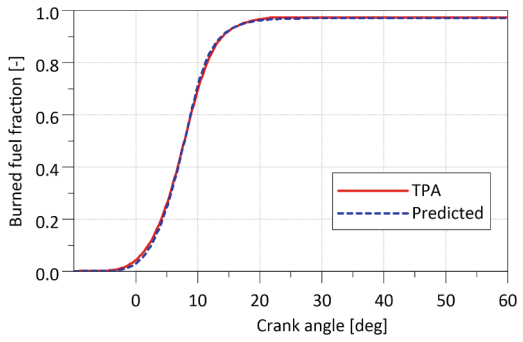

b. SGF burned fuel fraction, 1500 RPM, 9 bar IMEP, 0% EGR

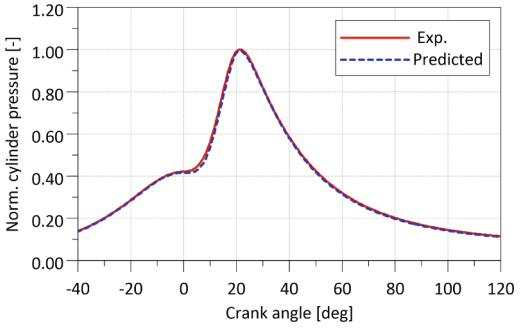

c. SGF in-cylinder pressure, 2500 RPM, 18 bar IMEP, 0% EGR

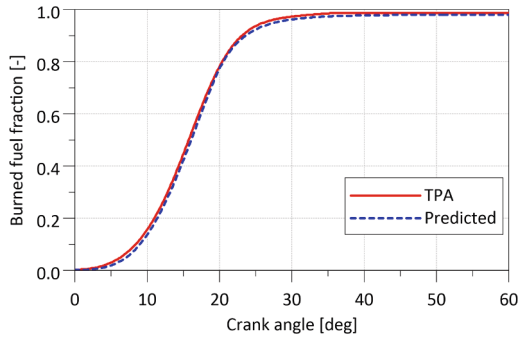

d. SGF burned fuel fraction, 2500 RPM, 18 bar IMEP, 0% EGR

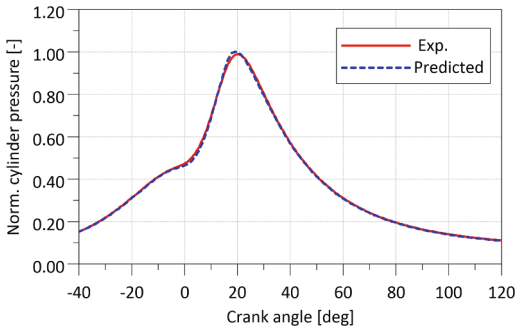

e. MtG – E10 in-cylinder pressure, 2500 RPM, 16 bar IMEP, 15% EGR

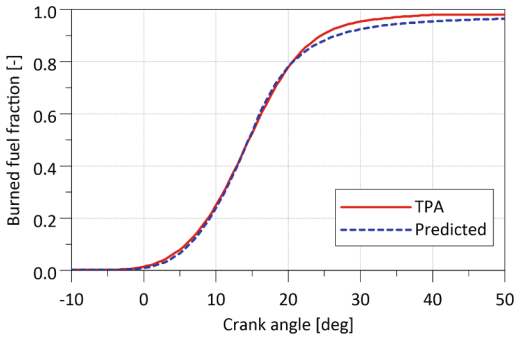

f. MtG – E10 burned fuel fraction, 2500 RPM, 16 bar IMEP, 15% EGR

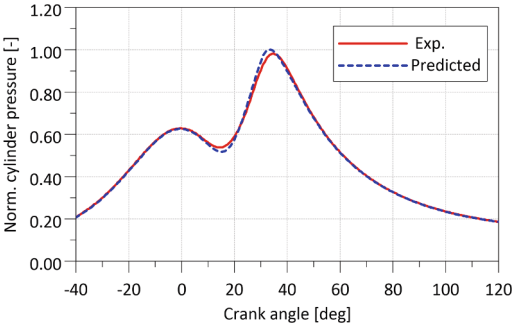

g. MtG – E10 in-cylinder pressure, 2500 RPM, 21 bar IMEP, 0% EGR

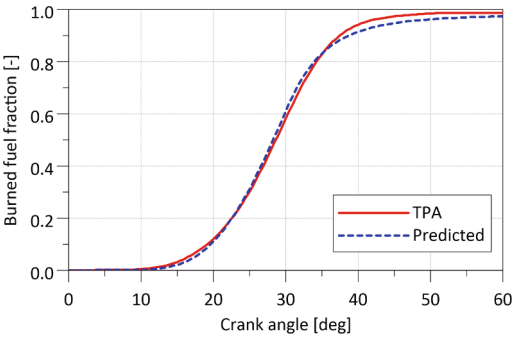

h. MtG – E10 burned fuel fraction, 2500 RPM, 21 bar IMEP, 0% EGR

Fig. 11. Predictive combustion model outcomes.

Table 14
Overall combustion metric quantities RMSE.

Variable	RMSE
IMEP [bar]	0.134
MFB50 [deg]	0.758
MFB1090 [deg]	1.182
Max. pressure [bar]	1.698
CA at max. pressure [deg]	0.948

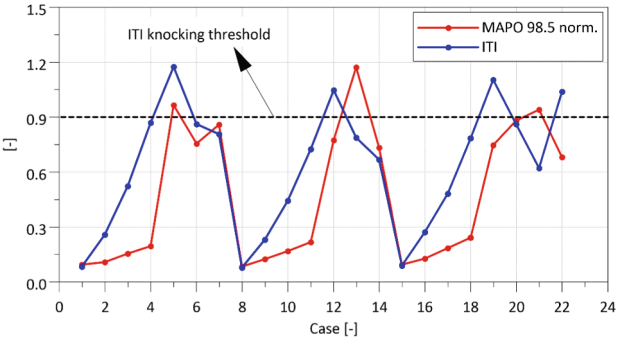

a. SGF

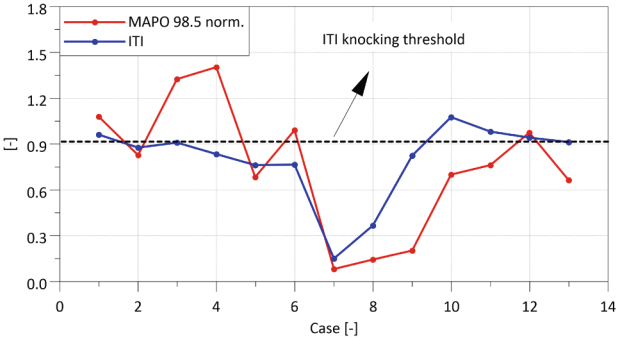

b. MtG – E10

Figure 12. Knock induction time integral and normalised $MAPO_{98.5}$ percentile

Fig. 12. Knock induction time integral and normalised $MAPO_{98.5}$ percentile.

to it, which is also confirmed by the ITI value. Capturing the knock occurrence for a 0D model is not straightforward, as knock onset is primarily influenced by local conditions within the cylinder that a 0D model cannot replicate. Moreover, being the real oxygenated compound in the SGF, different from ethanol, the behaviour of the fuel to auto-ignition could slightly deviate from the ETRF surrogate composition employed in this study. Overall, when examining all cases, the knocking trend is still successfully reproduced.

Coming to the MtG – E10 analysis, cases from 1 to 6 are characterised by IMEP = 16 bar and an EGR sweep from 0 to 25% at 2500 RPM. EGR affects the ignition delay of gas oil significantly, thanks to the oxygen reduction and high specific heat of carbon dioxide and water thermodynamic effect [71,72]. In this regard, the ITI shows a decreasing trend for such cases, while the normalised MAPO 98.5 percentile is always around or above 1, highlighting the fact that these cases are knocking ones or close to knocking. The 0D knock model for high EGR percentages does not predict the knocking occurrence; however, it is very close to the knocking threshold. Again, case 10 is run at 12 bar IMEP, and the same knocking prediction as for the SGF can be noticed. Cases from 11 to 13 are characterised by IMEP sweep from 15 to 21 bar at 2500 RPM, which are always knock-limited. The spark advance is adjusted to comply with the MAPO 98.5 percentile knock limit, and as a matter of fact, the value of the ITI remains almost constant for such engine OP_s.

5. Conclusions

This study focused on developing a fuel modelling methodology to extend an existing one-dimensional engine model – originally designed for fossil gasoline – to simulate combustion and knock dynamics of SI engines fuelled with e-gasoline. Fuel flexibility was achieved by integrating fuel-specific LFS and ID times into the model. The methodology was then validated using experimental data from an SCRE operated with MtG-E10 and another renewable synthetic fuel, referred to as SGF.

In order to account for the fuel chemical kinetics in the already calibrated predictive combustion model for standard RON95E10, an equivalent fuel composition, that is the surrogate fuel, was estimated. The implemented surrogate fuel algorithm aims to replicate fuel target properties, such as density, RON/MON, CHR, and VO, by using a hydrocarbon species palette, whose components' chemical kinetics have been thoroughly investigated in the literature.

To account for the dependency of LFS and ID on fuel composition, a grid of LFS and ID values, corresponding to different in-cylinder conditions, was generated for the fuel under analysis. The predictive combustion model was tailored according to each fuel by integrating an LFS neural network into the SI combustion template. The turbulent flame speed parameters were not recalibrated while switching fuel kinds.

Moreover, for the knock prediction, the Livengood-Wu knock induction time integral method was employed [41]. A simplified ETRF surrogate formulation was used in this regard, being the LLNL chemical reaction mechanism suitable to reproduce experimental ETRF ignition delays [70].

The predictive combustion model is able to reproduce the experimental in-cylinder pressure, as well as the burn rate of all the fuels, with high accuracy. As for the knock model, the general trend of the normalised MAPO 98.5 percentile by the empirical knock limit is replicated by the model's ITI across various engine operating conditions. The overall methodology is proven to be reliable for multiple fuel kinds, enabling the possibility of simulating the combustion of a general gasoline-like fuel and reducing the need for experimental data acquisition.

Future studies may involve the extension of the combustion model analysis to lean mixtures, which is of particular interest when direct fuel injection is addressed. Alternative synthetic fuel formulations also exhibit different evaporation behaviours, and further analysis would be required if air-mixture formation is investigated, particularly in a 3D CFD simulation framework.

Funding sources.

This research did not receive any specific grant from funding agencies in the public, commercial, or not-for-profit sectors.

CRediT authorship contribution statement

Lorenzo Ferrari: Writing – review & editing, Writing – original draft, Visualization, Validation, Software, Methodology, Investigation. **Massimo Duchi:** Writing – review & editing, Software, Methodology, Investigation. **Giuseppe Sammito:** Validation, Supervision, Project administration. **Bartosch Jagodzinski:** Validation, Supervision, Project administration, Data curation. **Nicolò Cavina:** Validation, Supervision, Software, Project administration.

Declaration of competing interest

The authors declare that they have no known competing financial interests or personal relationships that could have appeared to influence

the work reported in this paper.

Acknowledgments

The authors are thankful to Convergent Science for providing CONVERGE licenses.

Appendix

Table A1
Specifications of the test cell measurement instruments [21].

Instrument	Model	Measurement range	Accuracy
Engine dynamometer	Schorch	0–10,000 1/min	≤ 0.04%
Air mass flow meter	FEV air rate	0–1000 kg/h	≤ 1.00%
Fuel mass flow meter	Emerson Micro Motion Coriolis CMFS007	0–34.92 kg/h	≤ 0.054%
In-cylinder pressure transducers	Kistler 6044A	0–300 bar	≤ 0.13% at 30 bar ≤ 0.01% at 200 bar
Intake pressure transducers	Kistler 4045A	0–5 bar	≤ 0.3%
Exhaust pressure transducers	Kistler 4045A	0–5 bar	≤ 0.3%
Exhaust gas analyser			
CLD (NO_X)	Eco Physics nCLD 811 M	0–5000 ppm	≤ 1%
NDIR (CO, CO_2)	Rosemount NGA 2000	0–10% (CO) 0–20% (CO_2)	≤ 1%
PMD (O_2)	Rosemount NGA 2000	0–25%	≤ 1%
FID (HC)	Rosemount NGA 2000	10–10,000 ppm	≤ 1%
Particulate matter, soot	AVL 415SE smoke meter	0–10 FSN	0.0001 FSN

CLD = chemiluminescence detector, NDIR = non-dispersive infrared detector, PMD = paramagnetic detector, FID = flame ionization detector, THC = total-HC referred to propane (C3), FSN = filter smoke number.

Data availability

The data that has been used is confidential.

References

[1] K. Calvin et al., 'IPCC, 2023: Climate Change 2023: Synthesis Report. Contribution of Working Groups I, II and III to the Sixth Assessment Report of the Intergovernmental Panel on Climate Change [Core Writing Team, H. Lee and J. Romero (eds.)]. IPCC, Geneva, Switzerland.', Intergovernmental Panel on Climate Change (IPCC), Jul. 2023. doi: 10.59327/IPCC/AR6-9789291691647.
[2] Bilgili M, Tumse S, Nar S. Comprehensive Overview on the present State and Evolution of Global Warming, climate Change, Greenhouse Gasses and Renewable Energy. Arab J Sci Eng Nov. 2024;49(11):14503–31. https://doi.org/10.1007/s13369-024-09390-y.
[3] 'Delivering the European Green Deal - European Commission'. Accessed: Mar. 05, 2025. [Online]. Available: https://commission.europa.eu/strategy-and-policy/priorities-2019-2024/european-green-deal/delivering-european-green-deal_en.
[4] Pearson RJ, Turner JWG. 'Renewable Fuels', in Comprehensive Renewable Energy. Elsevier 2012:305–42. https://doi.org/10.1016/B978-0-08-087872-0.00522-9.
[5] S. Khalili, E. Rantanen, D. Bogdanov, and C. Breyer, 'Global Transportation Demand Development with Impacts on the Energy Demand and Greenhouse Gas Emissions in a Climate-Constrained World', Energies, vol. 12, no. 20, Art. no. 20, Jan. 2019, doi: 10.3390/en12203870.
[6] M. N. Uddin and F. Wang, 'Fuelling A Clean Future: A Systematic Review of Techno-Economic and Life Cycle Assessments in E-Fuel Development', Jul. 16, 2024. doi: 10.26434/chemrxiv-2024-rt918.
[7] Peng B-B, Fan Y, Xu J-H. Integrated assessment of energy efficiency technologies and CO2 abatement cost curves in China's road passenger car sector. Energy Convers Manag Feb. 2016;109:195–212. https://doi.org/10.1016/j.enconman.2015.11.064.
[8] J. A. García Sánchez, J. M. López Martínez, J. Lumbreras Martín, M. N. Flores Holgado, and H. Aguilar Morales, 'Impact of Spanish electricity mix, over the period 2008–2030, on the Life Cycle energy consumption and GHG emissions of Electric, Hybrid Diesel-Electric, Fuel Cell Hybrid and Diesel Bus of the Madrid Transportation System', Energy Convers. Manag., vol. 74, pp. 332–343, Oct. 2013, doi: 10.1016/j.enconman.2013.05.023.
[9] Meinrenken CJ, Lackner KS. Fleet view of electrified transportation reveals smaller potential to reduce GHG emissions. Appl Energy Jan. 2015;138:393–403. https://doi.org/10.1016/j.apenergy.2014.10.082.
[10] Sanguesa JA, Torres-Sanz V, Garrido P, Martinez FJ, Marquez-Barja JM. A Review on Electric Vehicles: Technologies and challenges. Smart Cities Mar. 2021;4(1):372–404. https://doi.org/10.3390/smartcities4010022.
[11] Kober T, et al. Perspectives of Power-to-X technologies in Switzerland: a White Paper. ETH Zurich Jul. 2019. https://doi.org/10.3929/ETHZ-B-000352294.
[12] 'Commission takes action for clean and competitive automotive sector', European Commission - European Commission. Accessed: Dec. 29, 2025. [Online]. Available: https://ec.europa.eu/commission/presscorner/detail/en/ip_25_3051.
[13] Ababneh H, Hameed BH. Electrofuels as emerging new green alternative fuel: a review of recent literature. Energy Convers Manag Feb. 2022;254:115213. https://doi.org/10.1016/j.enconman.2022.115213.
[14] Nemmour A, Inayat A, Janajreh I, Ghenai C. Green hydrogen-based E-fuels (E-methane, E-methanol, E-ammonia) to support clean energy transition: a literature review. Int J Hydrog Energy Sep. 2023;48(75):29011–33. https://doi.org/10.1016/j.ijhydene.2023.03.240.
[15] Dieterich V, Buttler A, Hanel A, Spliethoff H, Fendt S. Power-to-liquid via synthesis of methanol, DME or Fischer–Tropsch-fuels: a review. Energy Environ Sci Oct. 2020;13(10):3207–52. https://doi.org/10.1039/D0EE01187H.
[16] Dell'Aversano S, Villante C, Gallucci K, Vanga G, Di Giuliano A. E-Fuels: a Comprehensive Review of the Most Promising Technological Alternatives towards an Energy transition. Energies Aug. 2024;17(16):3995. https://doi.org/10.3390/en17163995.
[17] Ram V, Salkuti SR. An Overview of Major Synthetic Fuels. Energies Mar. 2023;16(6):2834. https://doi.org/10.3390/en16062834.
[18] Levine RB, Pinnarat T, Savage PE. Biodiesel production from Wet Algal Biomass through in Situ Lipid Hydrolysis and Supercritical Transesterification. Energy Fuels Sep. 2010;24(9):5235–43. https://doi.org/10.1021/ef1008314.
[19] Tarascon J-M, Armand M. Issues and challenges facing rechargeable lithium batteries. Nature Nov. 2001;414(6861):359–67. https://doi.org/10.1038/35104644.
[20] Guan J, et al. Development of reactor configurations for an electrofuels platform utilizing genetically modified iron oxidizing bacteria for the reduction of CO2 to biochemicals. J Biotechnol Mar. 2017;245:21–7. https://doi.org/10.1016/j.jbiotec.2017.02.004.
[21] C. Wouters et al., 'Evaluation of Synthetic Gasoline Fuels and Alcohol Blends in a Spark-Ignition Engine', SAE Int. J. Fuels Lubr., vol. 15, no. 3, pp. 04-15-03–0017, May 2022, doi: 10.4271/04-15-03-0017.
[22] Yarulina I, Chowdhury AD, Meirer F, Weckhuysen BM, Gascon J. Recent trends and fundamental insights in the methanol-to-hydrocarbons process. Nat Catal Jun. 2018;1(6):398–411. https://doi.org/10.1038/s41929-018-0078-5.
[23] Villforth J, Kulzer AC, Weißhaar A, Deeg H-P, Bargende M. 'The Influence of eFuel Formulation on Post Oxidation and Cold Start Emissions', in SAE Technical Paper Series, 400 Commonwealth Drive, Warrendale, PA. United States: SAE International Apr. 2021. https://doi.org/10.4271/2021-01-0632.
[24] M. Albrecht, H.-P. Deeg, D. Schwarzenthal, and P. Eilts, 'The Influence of Fuel Composition and Renewable Fuel Components on the Emissions of a GDI Engine', presented at the CO2 Reduction for Transportation Systems Conference, Jun. 2020, pp. 2020-37–0025. doi: 10.4271/2020-37-0025.

[25] M. Albrecht, H.-P. Deeg, D. Schwarzenthal, and P. Eilts, 'Investigations of the Emissions of Fuels with different Compositions and Renewable Fuel Components in a GDI Engine', presented at the WCX SAE World Congress Experience, Apr. 2020, pp. 2020-01–0285. doi: 10.4271/2020-01-0285.
[26] Rockstroh T, Floweday G, Yates A. Optimisation of synthetic gasoline blend recipes for use in modern charge boosted GDI engines. Fuel Dec. 2016;186:800–20. https://doi.org/10.1016/j.fuel.2016.09.001.
[27] E. Rossi et al., 'Experimental and Numerical Investigation for Improved Mixture Formation of an eFuel Compared to Standard Gasoline', presented at the 15th International Conference on Engines & Vehicles, Sep. 2021, pp. 2021-24–0019. doi: 10.4271/2021-24-0019.
[28] W. J. Pitz et al., 'Development of an Experimental Database and Chemical Kinetic Models for Surrogate Gasoline Fuels', presented at the SAE World Congress & Exhibition, Apr. 2007, pp. 2007-01–0175. doi: 10.4271/2007-01-0175.
[29] Grubinger T, Lenk G, Schubert N, Wallek T. Surrogate generation and evaluation of gasolines. Fuel Jan. 2021;283:118642. https://doi.org/10.1016/j.fuel.2020.118642.
[30] Andrae J, Johansson D, Björnbom P, Risberg P, Kalghatgi G. Co-oxidation in the auto-ignition of primary reference fuels and n-heptane/toluene blends. Combust Flame Mar. 2005;140(4):267–86. https://doi.org/10.1016/j.combustflame.2004.11.009.
[31] Morgan N, Smallbone A, Bhave A, Kraft M, Cracknell R, Kalghatgi G. Mapping surrogate gasoline compositions into RON/MON space. Combust Flame Jun. 2010;157(6):1122–31. https://doi.org/10.1016/j.combustflame.2010.02.003.
[32] Di Lorenzo M, Brequigny P, Foucher F, Mounaïm-Rousselle C. Validation of TRF-E as gasoline surrogate through an experimental laminar burning speed investigation. Fuel Oct. 2019;253:1578–88. https://doi.org/10.1016/j.fuel.2019.05.081.
[33] Sarathy SM, Farooq A, Kalghatgi GT. Recent progress in gasoline surrogate fuels. Prog Energy Combust Sci Mar. 2018;65:67–108. https://doi.org/10.1016/j.pecs.2017.09.004.
[34] Fontanesi S, et al. Impact of fuel surrogate formulation on the prediction of knock statistics in a single cylinder GDI engine. Int J Engine Res Mar. 2024;25(3):405–23. https://doi.org/10.1177/14680874231195742.
[35] Metghalchi M, Keck JC. Burning velocities of mixtures of air with methanol, isooctane, and indolene at high pressure and temperature. Combust Flame Jan. 1982;48:191–210. https://doi.org/10.1016/0010-2180(82)90127-4.
[36] Ö. L. Gülder, 'Correlations of Laminar Combustion Data for Alternative S.I. Engine Fuels', presented at the West Coast International Meeting and Exposition, SAE International, Aug. 1984. doi: 10.4271/841000.
[37] Sok R, Yamaguchi K, Kusaka J. Prediction of Ultra-Lean Spark Ignition Engine Performances by Quasi-Dimensional Combustion Model with a Refined Laminar Flame speed Correlation. J Energy Res Technol 2020;143(032306):Dec. https://doi.org/10.1115/1.4049127.
[38] Del Pecchia M, Pessina V, Berni F, d'Adamo A, Fontanesi S. Gasoline-ethanol blend formulation to mimic laminar flame speed and auto-ignition quality in automotive engines. Fuel Mar. 2020;264:116741. https://doi.org/10.1016/j.fuel.2019.116741.
[39] A. D'Adamo, M. Del Pecchia, S. Breda, F. Berni, S. Fontanesi, and J. Prager, 'Chemistry-Based Laminar Flame Speed Correlations for a Wide Range of Engine Conditions for Iso-Octane, n-Heptane, Toluene and Gasoline Surrogate Fuels', presented at the International Powertrains, Fuels & Lubricants Meeting, Oct. 2017, pp. 2017-01–2190. doi: 10.4271/2017-01-2190.
[40] Sok R, Kataoka H, Kusaka J, Miyoshi A, Reitz RD. A novel laminar flame speed equation for quasi-dimensional combustion model refinement in advanced, ultra-lean gasoline spark-ignited engines. Fuel Feb. 2023;333:126508. https://doi.org/10.1016/j.fuel.2022.126508.
[41] Livengood JC, Wu PC. Correlation of autoignition phenomena in internal combustion engines and rapid compression machines. Symp Int Combust Jan. 1955;5(1):347–56. https://doi.org/10.1016/S0082-0784(55)80047-1.
[42] Ahmed A, Goteng G, Shankar VSB, Al-Qurashi K, Roberts WL, Sarathy SM. A computational methodology for formulating gasoline surrogate fuels with accurate physical and chemical kinetic properties. Fuel Mar. 2015;143:290–300. https://doi.org/10.1016/j.fuel.2014.11.022.
[43] Kim D, Song J, Song H, Lim Y, Lee S, Song HH. Assessment of hydrocarbons for gasoline surrogate: an optimization study. Fuel Nov. 2022;328:125286. https://doi.org/10.1016/j.fuel.2022.125286.
[44] F. Bozza, V. De Bellis, and A. Dulbecco, 'Advanced 0D and QuasiD Thermodynamic Combustion Models for SI and CI Engines', USA, 2020. Accessed: Mar. 07, 2025. [Online]. Available: https://www.iris.unina.it/handle/11588/952729.2.
[45] 'EN ISO 5164:2014 Petroleum products —Determination of knockcharacteristics of motor fuels— Research method.' 2014.
[46] 'EN ISO 5163:2014 Petroleum products —Determination of knockcharacteristics of motor andaviation fuels — Motor method. 2014'. 2014.
[47] R. Isermann, Engine Modeling and Control: Modeling and Electronic Management of Internal Combustion Engines. Berlin, Heidelberg: Springer Berlin Heidelberg, 2014. doi: 10.1007/978-3-642-39934-3.
[48] J. G. Speight, 'Chapter 10 - Combustion of Hydrocarbons', in Handbook of Industrial Hydrocarbon Processes, J. G. Speight, Ed., Boston: Gulf Professional Publishing, 2011, pp. 355–393. doi: 10.1016/B978-0-7506-8632-7.10010-6.
[49] Kroyan Y, Wojcieszyk M, Kaario O, Larmi M, Zenger K. Modeling the end-use performance of alternative fuels in light-duty vehicles. Energy Aug. 2020;205:117854. https://doi.org/10.1016/j.energy.2020.117854.
[50] Kroyan Y, Wojcieszyk M, Kaario O, Larmi M. Modelling the end-use performance of alternative fuel properties in flex-fuel vehicles. Energy Convers Manag Oct. 2022;269:116080. https://doi.org/10.1016/j.enconman.2022.116080.
[51] Huber ML, Lemmon EW, Bell IH, McLinden MO. The NIST REFPROP Database for Highly Accurate Properties of Industrially Important Fluids. Ind Eng Chem Res Oct. 2022;61(42):15449–72. https://doi.org/10.1021/acs.iecr.2c01427.
[52] 'EN 228:2012 Automotive fuels — Unleaded petrol —Requirements and test methods.' 2012.
[53] Sarathy SM, et al. Compositional effects on the ignition of FACE gasolines. Combust Flame Jul. 2016;169:171–93. https://doi.org/10.1016/j.combustflame.2016.04.010.
[54] Daly SR, Niemeyer KE, Cannella WJ, Hagen CL. FACE gasoline Surrogates Formulated by an Enhanced Multivariate Optimization Framework. Energy Fuels Jul. 2018;32(7):7916–32. https://doi.org/10.1021/acs.energyfuels.8b01313.
[55] J. E. Anderson et al., 'Octane Numbers of Ethanol-Gasoline Blends: Measurements and Novel Estimation Method from Molar Composition', presented at the SAE 2012 World Congress & Exhibition, Apr. 2012, pp. 2012-01–1274. doi: 10.4271/2012-01-1274.
[56] Mariani V, Pulga L, Bianchi GM, Falfari S, Forte C. Machine Learning-based Identification strategy of fuel Surrogates for the CFD simulation of Stratified Operations in Low Temperature Combustion Modes. Energies Jul. 2021;14(15):4623. https://doi.org/10.3390/en14154623.
[57] Ugray Z, Lasdon L, Plummer J, Glover F, Kelly J, Marti R, et al. Social Science Research Network. Rochester, NY 2006;886559. https://doi.org/10.2139/ssrn.886559.
[58] S. Demesoukas, C. Caillol, P. Higelin, and A. Boiarciuc, 'Zero-Dimensional Spark Ignition Combustion Modeling - A Comparison of Different Approaches', presented at the 11th International Conference on Engines & Vehicles, Sep. 2013, pp. 2013-24–0022. doi: 10.4271/2013-24-0022.
[59] Peters N. Laminar flamelet concepts in turbulent combustion. Symp Int Combust Jan. 1988;21(1):1231–50. https://doi.org/10.1016/S0082-0784(88)80355-2.
[60] Sileghem L, et al. Laminar burning velocity of gasoline and the gasoline surrogate components iso-octane, n-heptane and toluene. Fuel Oct. 2013;112:355–65. https://doi.org/10.1016/j.fuel.2013.05.049.
[61] Hu E, Ku J, Yin G, Li C, Lu X, Huang Z. Laminar Flame Characteristics and Kinetic Modeling Study of Ethyl Tertiary Butyl Ether Compared with Methyl Tertiary Butyl Ether, Ethanol, iso-Octane, and gasoline. Energy Fuels Mar. 2018;32(3):3935–49. https://doi.org/10.1021/acs.energyfuels.7b03636.
[62] Ranzi E, Frassoldati A, Stagni A, Pelucchi M, Cuoci A, Faravelli T. Reduced Kinetic Schemes of complex Reaction Systems: Fossil and Biomass-Derived Transportation Fuels. Int J Chem Kinet Sep. 2014;46(9):512–42. https://doi.org/10.1002/kin.20867.
[63] 'Richards, K.J., Senecal, P.K., and Pomraning, E., CONVERGE 4.1, Convergent Science, Madison, WI (2025).'.
[64] Pera C, Knop V. Methodology to define gasoline surrogates dedicated to auto-ignition in engines. Fuel Jun. 2012;96:59–69. https://doi.org/10.1016/j.fuel.2012.01.008.
[65] Gauthier BM, Davidson DF, Hanson RK. Shock tube determination of ignition delay times in full-blend and surrogate fuel mixtures. Combust Flame Dec. 2004;139(4):300–11. https://doi.org/10.1016/j.combustflame.2004.08.015.
[66] Andrae JCG, Björnbom P, Cracknell RF, Kalghatgi GT. Autoignition of toluene reference fuels at high pressures modeled with detailed chemical kinetics. Combust Flame Apr. 2007;149(1–2):2–24. https://doi.org/10.1016/j.combustflame.2006.12.014.
[67] Andrae JCG, Head RA. HCCI experiments with gasoline surrogate fuels modeled by a semidetailed chemical kinetic model. Combust Flame Apr. 2009;156(4):842–51. https://doi.org/10.1016/j.combustflame.2008.10.002.
[68] Andrae JCG. Comprehensive chemical kinetic modeling of toluene reference fuels oxidation. Fuel May 2013;107:740–8. https://doi.org/10.1016/j.fuel.2013.01.070.
[69] Dirrenberger P, et al. Laminar burning velocity of gasolines with addition of ethanol. Fuel Jan. 2014;115:162–9. https://doi.org/10.1016/j.fuel.2013.07.015.
[70] Mehl M, Pitz WJ, Westbrook CK, Curran HJ. Kinetic modeling of gasoline surrogate components and mixtures under engine conditions. Proc Combust Inst Jan. 2011;33(1):193–200. https://doi.org/10.1016/j.proci.2010.05.027.
[71] Kobashi Y, Todokoro M, Shibata G, Ogawa H, Mori T, Imai D. EGR gas composition effects on ignition delays in diesel combustion. Fuel Dec. 2020;281:118730. https://doi.org/10.1016/j.fuel.2020.118730.
[72] Cai L, Ramalingam A, Minwegen H, Alexander Heufer K, Pitsch H. Impact of exhaust gas recirculation on ignition delay times of gasoline fuel: an experimental and modeling study. Proc Combust Inst 2019;37(1):639–47. https://doi.org/10.1016/j.proci.2018.05.032.